JOURNAL OF MATERIALS SCIENCE 30 (1995) 4161–4170

Characterizing the cross-sectional geometry of thin, non-cylindrical, twisted fibres (spider silk)

D. L. DUNAWAY, B. L. THIEL*, S. G. SRINIVASAN*, C. VINEY‡
*Molecular Bioengineering Program, Center for Bioengineering WD-12, and *Department of Materials Science and Engineering FB-10, University of Washington, Seattle, WA 98195, USA*

Quantitative tensile property evaluation of fibres requires accurate cross-sectional area measurement at a location close to the point of failure. Laser diffraction was evaluated as a non-destructive technique for characterizing the cross-sectional geometry of translucent, non-cylindrical, and/or twisted fibres with thicknesses in the range 2–5 μm. Forcibly silked major ampullate fibres from *Nephila clavipes* spiders were used as specimens. Scanning electron microscopy was used to calibrate the extent to which laser diffraction over- or under-estimates fibre diameter. For the purpose of area measurement, elliptical or oval cross-sections can be treated as though they were circular. We demonstrate mathematically that the area can be obtained to within a few per cent of the true value, if (a) the circle is assigned an "equivalent diameter" equal to the average of at least four measurements of apparent diameter, (b) the apparent diameter measurements are taken at equal intervals of fibre rotation through a 180° range, and (c) the axial ratio of the cross-section is less than 1.5. The extent to which a non-cylindrical fibre is twisted can be deduced from the periodicity of bright and dark regions that alternate along the length of the fibre in reflected light. Values of cross-sectional ellipticity and area measured from a twisted fibre were smaller than the corresponding values obtained from a twist-free fibre. The apparent diameter of twist-free major ampullate fibre was found to be highly variable – by as much as ±20% relative to the mean within a 0.6 mm length. Therefore, local measurements of area, rather than a value derived from fibre denier, should be used in tensile property evaluation of this material.

1. Introduction

Spider major ampullate silk, which forms the thicker pair of strands in dragline and web frame silk, exhibits an impressive spectrum of tensile properties [1–3]. These include strength, stiffness and toughness, all of which can be quantified from stress–strain curves. The accurate determination of these properties requires reliable values of fibre cross-sectional area. However, the cross-sectional geometry of major ampullate silk is difficult to characterize, because the thickness of these fibres (typically 1–5 μm for mature spiders [2, 4, 5]) is significantly less than that of conventional textile fibres. This paper discusses the merits and limitations of laser diffraction as applied to measuring the cross-sectional area of fine fibres, specifically natural silk.

A robust technique for measuring fibre cross-section should ideally be non-destructive, so that measurements can be taken at any step in fibre processing. The technique should be able to accommodate the measurement of fibres that are not cylindrical, i.e. that do not have a circular cross-section. Finally, the technique should yield a usable and reliable result in a minimum of time. Three techniques are commonly used for fibre diameter characterization: light microscopy with an image shearing eyepiece [6, 7], scanning electron microscopy (SEM) [8], and laser diffraction [8–12]. Only the last technique meets the stated criteria. Light microscopy is destructive, because oil immersion is required to achieve the resolution necessary for accurately measuring the diameter of thin fibres. In addition, light microscopy provides only an "apparent" diameter, i.e. the width of the fibre as presented to the specific viewing direction. SEM is more accurate than light microscopy, and can also characterize diameter variations on a smaller scale along the length of the fibre. However, the practically achievable range of viewing directions is still restricted, and the process of mounting the specimens for SEM [8] is destructive. Laser diffraction is non-destructive and precise [10]; it can provide cross-sectional area and shape information in some circumstances [9], and it is accurate if calibrated by another method such as SEM [8].

2. Background

2.1. Fraunhofer approximation for fibres

If a cylindrical, opaque fibre is illuminated by parallel light (equivalent to a light source at infinity),

‡Author to whom all correspondence should be addressed.
Present address (permanent): University of Oxford, Department of Materials, Parks Road, Oxford OX1 3PH, UK.

0022–2461

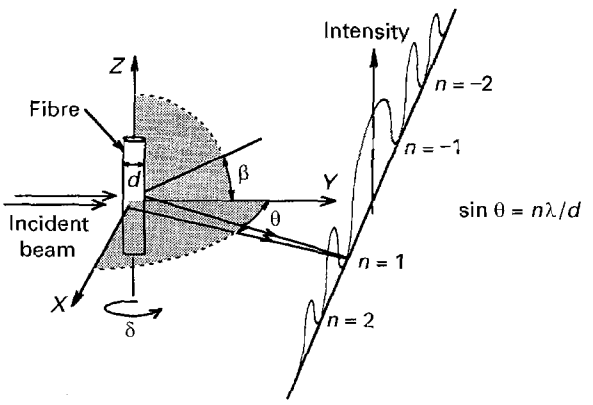

Figure 1 Fraunhofer diffraction by a fibre. Schematic illustration defining laboratory axes, X, Y, Z, fibre rotation, δ, and diffraction angles, θ, β.

a Fraunhofer diffraction pattern can be observed by placing a screen at a large distance (compared to the fibre diameter and to the wavelength of the light) beyond the fibre (Fig. 1). The intensity of the diffracted radiation at a given point in the pattern depends on the diffraction angle, θ, because the extent of constructive or destructive interference between light diffracted at opposite sides of the fibre depends on the difference in path length to that point. To a first approximation, the same diffraction pattern can be obtained by replacing the fibre with a transparent glass slide on which is painted an opaque strip having a width equal to the fibre diameter, d. Following Babinet's principle [13], this diffraction pattern could also be obtained by replacing the fibre with an opaque sheet into which is cut a transparent slit having a width equal to the fibre diameter. On this basis, the angular location of the regions of destructive interference (or nodes) for single-fibre diffraction is described by the same equation that pertains to Fraunhofer diffraction by a single rectangular slit. For a given wavelength, λ, of radiation

$$\sin\theta = \frac{n\lambda}{d} \tag{1}$$

where n is an integer. Usually, the first-order node ($n = 1$) is used in diameter measurements, because the local contrast in the diffraction pattern is greater than at the higher-order nodes.

The Fraunhofer approximation does not completely match experimental diffraction patterns, but with a correction for systematic error the technique has been shown to be highly accurate [8] for opaque fibres. Correction factors obtained by SEM have been published [8], but these data only extend down to fibre diameters of 5 μm, which is too coarse for most spider silk. Also, silk fibres are translucent. Because the difference in refractive index between the fibre and the surrounding medium affects the diffraction angles associated with nodes [14, 15], a separate calibration should be conducted for each translucent material. While the diffraction of light by spider webs has been discussed previously [16], this was not done with the goal of fibre diameter measurement.

2.2. Non-cylindrical and twisted fibres

Silkworm cocoon silk fibres have a roughly triangular cross-section [17, 18]. There is limited evidence that the cross-section of major ampullate spider silk depends on the conditions under which the fibres are spun. Light microscopy [19] and transmission electron microscopy [5] suggest that forcibly silked fibres have an elliptical cross-section, while web fibres exhibit a circular cross-section as observed by SEM [19]. We note that there is nothing intrinsic to the shape of spider or insect spinnerets that suggests natural silk fibres should be cylindrical.

Li and Tietz [8] suggest (though without demonstration or discussion) that the area of a non-cylindrical fibre can be accurately calculated by assuming that the fibre cross-section *is* circular, and using an "equivalent diameter" obtained by averaging a number of measurements taken as the fibre is rotated about its long axis. However, non-cylindrical fibres that additionally are fine, twisted and translucent, present special problems that the literature does not address. This paper describes how, and to what level of accuracy, cross-sectional area can be measured in such cases, down to fibre diameters of 2 μm.

It has been shown that *twisted* elliptical fibres exhibit diffraction patterns in which the intensity variation is two-dimensional [20]. The pattern perpendicular to the fibre (θ plane; Fig. 1) is related to the fibre width as sampled by the diffracted rays. The pattern parallel to the fibre (β plane) is related to the frequency of macroscopic structural repeats induced by twisting the fibre, and to δ, the rotation of the fibre about its long axis. The pattern in the β plane depends upon ν, the number of structural repeats sampled by the laser beam, as follows

$$\nu = \frac{D}{l} \tag{2}$$

where D is the diameter of the beam and l is the length per structural repeat. In other words, l is the length over which a 180° twist occurs and is equal to $L/(2N)$, where L is the length of the fibre and N is the total number of full twists. Bickel *et al.* [20] mistakenly place the factor of 2 in the numerator; however, it should be in the denominator. (Given two repeats per twist, the length per repeat should decrease instead of increase with inclusion of this factor.)

3. Experimental procedure

3.1. Sample preparation

Single major ampullate fibres were drawn from mature specimens of the spider *Nephila clavipes* at 10.3 cm s^{-1} following a procedure described by Work and Emerson [21]. The samples were stored in a desiccator at room temperature before use. Sections of fibres were glued with Devcon 5 minute epoxy (Devcon Corporation, Danvers, MA) on to notched glass slides, so that fibres were suspended without slack across the 0.5 in × 0.75 in (1.27 cm × 1.9 cm) opening (Fig. 2). Specimens have to be dust-free, because dust particles degrade the fibre diffraction pattern, making it difficult to locate the nodes [8].

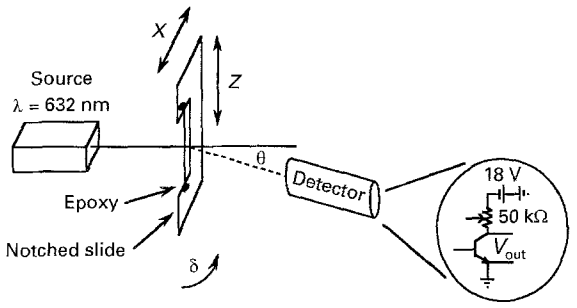

Figure 2 Apparatus used to characterize fibre diameter from a Fraunhofer diffraction pattern. Specimens are mounted on a rotatable platform, δ, which in turn is mounted on horizontal, X, and vertical, Z, translation stages.

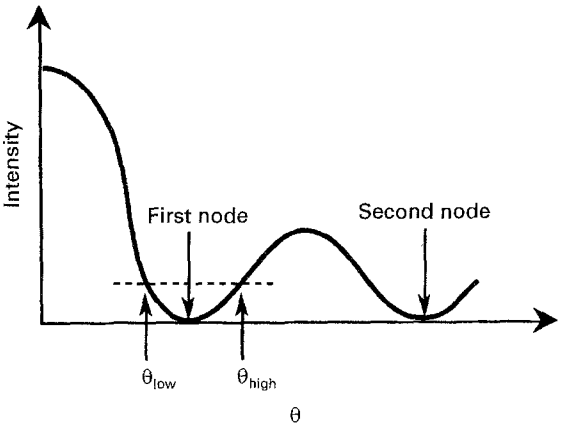

Figure 3 Schematic representation of measurements, θ_{low} and θ_{high}, used to locate the diffraction angle, $(\theta_{low} + \theta_{high})/2$, that corresponds to the first node. Typically, the angular separation between θ_{low} and θ_{high} was 3% of the angular separation between the first and second nodes. Within experimental resolution, the curves of intensity versus diffraction angle were always symmetrical about the first node over at least the range θ_{low} to θ_{high}.

3.2. Apparatus

Laser diffraction has been employed to measure the diameter of many different types of fibres, but the literature does not address fibres that are as fine as silk. Typically, the Fraunhofer diffraction patterns are displayed on a flat vertical surface (e.g. a wall) and the nodes (intensity minima) are located visually [8, 10]. The fibre diameter can then be calculated from the measured separation of the nodes and the known distance from the fibre to the wall. With decreasing fibre diameter, the diffraction angles for the nodes are increased. For example, the diffraction angle to the $n = 1$ node is 7.3° when $\lambda = 0.632$ μm light is diffracted by a 5 μm diameter fibre, and this angle increases to 39° for a 1 μm diameter fibre. When the diffraction pattern is broadened in the θ plane in the way, it becomes increasingly difficult to locate the intensity minima visually. While a shorter illuminating wavelength (e.g. use of ultraviolet light) could alleviate this problem, this would increase the risk of damage to the protein backbone of silk [22]. Another drawback associated with large diffraction angles, is that rays reflected from the fibre interfere with the diffraction pattern, which again complicates the detection of nodes [23]. Non-circular fibres cause additional degradation of the pattern in both the θ and β planes. The precision and reproducibility with which nodes are located can be improved by electronic detection [9].

The apparatus (Fig. 2) used to measure the angular separation of nodes was a modified ellipsometer, similar to the setup used by Gagnaire *et al.* [9]. The light source was a 632 nm, 3.0 mW HeNe laser (05 LLP 831; Melles Griot, Irvine, CA) with a nominal beam diameter of 0.59 mm and a 1.3 mrad divergence. The slide with the fibre sample was mounted on the ellipsometer, and manipulated by X (horizontal translation), Z (vertical translation) and δ (rotation) stages, all of which could be controlled remotely. The detector was motorized so that rotation through the angle θ could be accomplished in a way that eliminated the manual repetitiveness of these measurements. A photodarlington transistor (NTE3036), in common emitter configuration, measured the light intensity (Fig. 2). The output voltage was measured by a Beckman Industrial DM78 digital multimeter. Because some of the nodes are less distinct than others, the sensitivity of the circuit had to be adjusted by changing the setting of the 50 kΩ variable resistor.

3.3. Measurements

3.3.1. Location of nodes

The diffraction pattern was scanned by sweeping the detector in the θ plane, to locate intensity minima. The nodes were often difficult to locate directly, because the intensity varies slowly with diffraction angle near the centre of a node. Therefore, minima were located by identifying points of identical intensity on either side of the node (where intensity varies more rapidly with diffraction angle) and averaging their diffraction angles (Fig. 3).

3.3.2. Modelling the fibre cross-section

Given that we are measuring fibre diameter in an effort to obtain reliable values of cross-sectional area, the following practical questions must be addressed. First: is it appropriate to treat elliptical fibres as though they have a circular cross-section and to obtain an "equivalent" diameter by averaging several measurements performed on the ellipse, or should one instead take several diameter measurements around a fibre and fit an ellipse? Second: to what extent does the answer to the previous question depend on the number and angular separation of the individual diameter measurements that are made? It can be shown that the errors in cross-sectional area measurement are small when fibres are assigned a circular cross-section, provided that the equivalent diameter is calculated from at least four measurements taken at equal intervals of fibre rotation through a 180° range. The details of the mathematical treatment are presented in the Appendix.

3.3.3. Asymmetric diffraction patterns

If fibres have a circular cross-section, the diffraction angle has the same magnitude for equivalent nodes

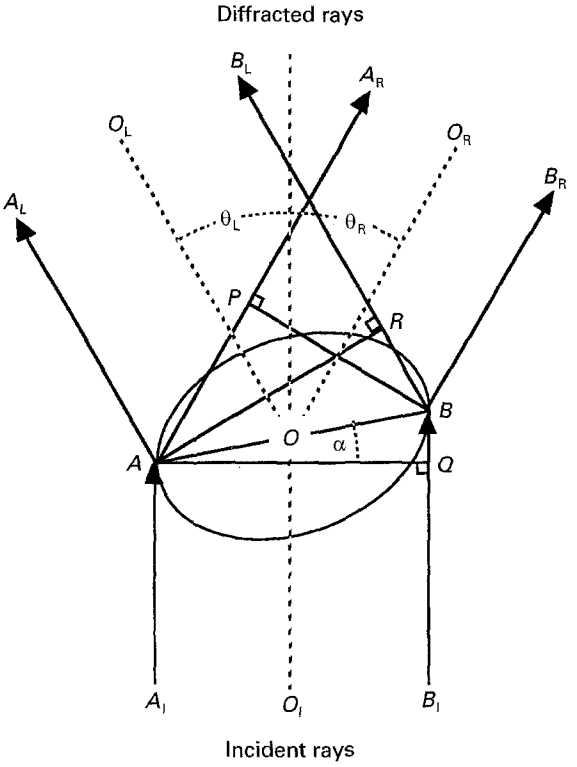

Figure 4 Geometry referenced in qualitative discussion of Fraunhofer diffraction by fibres that have an elliptical cross-section. To a first approximation, ray paths are assumed to be unaffected by the refractive index difference between the fibre and air.

($n = \pm n_i$) on either side of the direct beam [8]. In such cases, the angular separation of equivalent nodes can be interpreted straightforwardly in terms of fibre diameter. However, fibres with non-circular cross-sections will, in general, give rise to asymmetric diffraction patterns, in which equivalent nodes do not appear at the same diffraction angle on either side of the direct beam. This phenomenon can be described qualitatively with reference to Fig. 4, which shows a fibre with an elliptical cross-section. Because the fibre is non-cylindrical, the apparent diameter, $\overline{AQ}$, sampled by diffraction, corresponds to an actual diameter, $\overline{AB}$, that is skewed by the angle, α, from lying transverse to the incident beam. Unless $\alpha = \pi m$ (where m is an integer), $\overline{AB}$ explicitly does *not* correspond to a principal axis of the elliptical fibre cross-section. Let us assume that θ_L corresponds to the first node on the left of the direct beam, i.e. the rays $A_I A_L$ and $B_I B_L$ combine to give destructive interference. If the diffraction pattern is to be symmetric, then $\theta_R = \theta_L$ must also correspond to a node in the diffraction pattern, in which case the path difference for rays $A_I A_R$ and $B_I B_R$ must equal the path difference for rays $A_I A_L$ and $B_I B_L$. To a first approximation (disregarding factors such as the limited fibre transparency, the refractive index difference between the fibre and air, and the optical anisotropy of the fibre, this requires

$$\overline{QB} + \overline{BR} = \overline{AP} - \overline{QB} \quad (3)$$

The individual segment lengths in Equation 3 can be expressed as follows

$$\overline{QB} = \overline{AB}\sin\alpha \quad (4)$$

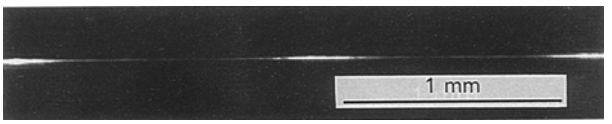

Figure 5 Pattern of reflected light exhibited by a twisted fibre of *N. clavipes* major ampullate silk. Although the periodic nature of the pattern can be observed with the naked eye, a microscope (× 40 dry objective) was used to obtain the image shown here, to facilitate recording of the intensity variation along the length of the fibre. A Microtek ScanMaker 600ZS scanner and Adobe Photoshop image processing software were used to generate a digital image from a printed micrograph.

$$\overline{BR} = \overline{AB}\sin(\theta_L - \alpha) \quad (5)$$

$$\overline{AP} = \overline{AB}\sin(\theta_L + \alpha) \quad (6)$$

Substitution of Equations 4–6 into Equation 3, followed by some simplification, yields the special cases under which equivalent nodes are located symmetrically relative to the direct beam

$$(1 - \cos\theta_L)\sin\alpha = 0 \quad (7)$$

This corresponds to the trivial case of $\theta_L = 2\pi m$ (m is an integer), and to the special rotations of the fibre defined by $\alpha = \pi m$. The general asymmetry ($\theta_L \neq \theta_R$) of diffraction patterns associated with non-cylindrical cross-sections is more apparent in the case of fine fibres, because diffraction angles are larger, and the geometrical path differences $\overline{QB} + \overline{BR}$ (left-hand side of Equation 3) and $\overline{AP} - \overline{QB}$ (right-hand side of Equation 3) become increasingly dissimilar.

We performed experiments on several fibres to determine how equivalent diameter (calculated from four measurements of apparent diameter taken at 45° intervals of fibre rotation; Appendix) depends on which of θ_L, θ_R, or $(\theta_L + \theta_R)/2$ is used in Equation 1 to find individual values of apparent diameter. These experiments demonstrated that the three methods yield results differing by no more than 2%, and that this difference arises as a systematic error when the laser and detector are not properly aligned at $\theta = 0$. The effect of the systematic error is greater for thicker fibres, because diffraction angles are smaller and any misalignment is a larger fraction of the measurement. It is minimized when the average of θ_L and θ_R is used in Equation 1 to measure apparent diameters.

3.3.4. Investigating the effect of fibre twist

During specimen handling, it was noticed that some fibres exhibit periodic patterns of reflected light along their length (Fig. 5). Such light and dark banding is consistent with the development of twist in a non-cylindrical fibre. To investigate the effect of fibre twist on banding and on the diffraction patterns, small weights were suspended from a single silk fibre and a single strand of hair; the latter material was included to determine if the banding phenomenon occurs in fibres other than silk. The weights could be turned easily to induce twists in the fibre, in a manner similar to that used by Bickel *et al.* [20]. This device was placed on the ellipsometer translation/rotation stage,

and each fibre was characterized to determine whether changes in the value of v (Equation 2) affect the measurement of diameter.

3.3.5. Calibration of diffraction versus SEM for diameter measurement

The silk used for calibration purposes was drawn from three different spiders on different days in an attempt to obtain a range of fibre diameters. The equivalent diameter of specimens was first characterized by laser diffraction, using six measurements of apparent diameter taken at 30° intervals of fibre rotation. Each fibre was then centred on an SEM stub and held with an adhesive graphite tab. As a calibration standard, polystyrene spheres (Ted Pella, Redding, CA; mean diameter 0.730 μm, standard deviation ± 0.001 μm) were sprinkled across the stub. The specimen and stub were sputtered with a thin Au–Pd coating. Specimens were observed in a JEOL JSM 6300F field-emission SEM, at a working distance of 15 mm and with an accelerating voltage of 3 kV. Three micrographs of the central region of the fibre were taken to cover the nominal 0.6 mm diameter region previously sampled with the laser beam. The apparent specimen diameter was measured at the top, middle, and bottom of each micrograph. These nine values were used to calculate an average that could be compared to the equivalent diameter obtained from laser diffraction. Specimens that were markedly non-cylindrical (as revealed by laser diffraction) or that exhibited a highly non-uniform diameter along their length (as revealed in the SEM) were excluded from the calibration.

4. Results and discussion

4.1. Observation of fibre twist

The periodic pattern of light and dark bands exhibited in reflected light by many major ampullate silk fibres (and also hair) can be altered by manual twisting. An increase in the amount of twist is accompanied by an increase in the number, and a decrease in the separation, of the bright bands. The phenomenon can be observed with the unaided eye if the fibre is viewed under sufficiently oblique illumination, enabling easy measurement of the quantity v in Equation 2. The fact that the bands are not equally distinct on all fibres is consistent with the fibres having different cross-sectional aspect ratios: fibres with nearly circular cross-sections will exhibit the most poorly-defined bands.

We have not conclusively identified the cause of the twist in forcibly silked major ampullate fibres. However, we have observed that the number of twists per unit length of fibre is decreased at higher rates of forced silking, which generate a greater degree of axial restraint than low rates of silking. It is well known [24] that moisture can cause macroscopic distortion and microscopic changes of crystallite orientation in major ampullate silk, and that these effects depend on the extent of axial restraint being applied. Therefore, we suggest a role either for atmospheric moisture, or for water retained from the original secretion, in causing the observed twist of forcibly silked fibres. Supporting evidence is provided by the observation that fibres are less twisted after they have been placed in a vacuum and Au–Pd sputtered, i.e. subjected to a treatment in which they are dried and then sealed with a moisture-resistant coating.

TABLE I The effect of fibre twist on the ellipticity and cross-sectional area measured by laser diffraction

v	ε, ellipticity	d_{eq} (μm)	Area from d_{eq} (μm^2)
0	1.5	4.47	15.7
0.05	1.5	4.47	15.7
0.1	1.5	4.43	15.4
0.2	1.5	4.45	15.6
0.4	1.2	4.43	15.4
0.7	1.3	4.35	14.9
1.0	1.1	4.4	15.2
1.5	1.0	4.34	14.8

4.2. Area and shape information

Table I lists measurements that were made on a fibre mounted so that the value of v could be changed without affecting the Z position of the fibre within the laser beam. Five measurements of apparent diameter, taken at 36° intervals of fibre rotation δ, were averaged to calculate equivalent diameters (Equation A11) for v values between 0 and 1.5. These equivalent diameters were used to calculate corresponding values of cross-sectional area (Equation A12). The apparent diameter measurements were also plotted in a polar format (similar to Fig. A3) for each v value. A value of ellipticity (ε, length-to-width ratio of cross-section) was estimated from each polar plot.

The ε values tend to decrease towards 1 with increasing v. As the fibre becomes more twisted, the laser beam samples an increasingly complete range of the possible apparent diameters of the fibre during a single reading. In such cases, changing the rotation of the fibre between readings does not present a significantly different range of apparent diameters to the laser, and the specimen behaves as though it were approximately cylindrical. Thus, because the apparent diameter varies along the length sampled by the beam, the local shape of twisted fibres cannot be determined with laser diffraction. In order for laser diffraction to provide information on the shape of fibre cross-sections, the length that interacts with the beam must be free from twists and also constant in cross-sectional shape. The banded pattern of light reflected by the fibre can be used to assess the extent of twisting.

The cross-sectional area determined from diffraction measurements decreases slowly as a function of increasing fibre twist; the area at v = 1.5 is approximately 6% less than the area at v = 0. This decrease in measured diameter is a direct consequence of the decreased ellipticity and the three-dimensional shape change (curl) that is caused by the twist. Again, the extent of twisting can be evaluated from the pattern of reflected light, enabling some assessment of whether a cross-sectional area measurement will be reliable.

4.3. Calibration of laser diffraction versus SEM

The SEM characterization would ideally be performed on an end view of the fibre. However, this is precluded by the need first to maintain a sufficient length of twist-free and rotatable fibre for characterization by laser diffraction, and by the difficulties of subsequently breaking the fibre in the right place and without introducing unwanted deformation.

Laser diffraction effectively samples a continuum of apparent diameters over the nominal 0.6 mm length of fibre that crosses the beam. This distance corresponds to 120 diameters (0.6 mm/0.005 mm) for a 5 μm thick fibre, and 300 diameters (0.6 mm/0.002 mm) for a 2 μm thick fibre. In contrast, the SEM values are averages of a small number of discrete diameter measurements made within the same 0.6 mm length. Most of the thinner fibres (2–4 μm) were highly variable in apparent diameter; in some cases, individual SEM measurements of diameter varied over as much as a ± 20% range relative to the mean within this length. Optimally, the calibration to assess the level of agreement between the two techniques would be performed on fibres that have a constant diameter, but none of our material was that uniform. As a compromise, specimens were excluded from the calibration if the coefficient of variation (standard deviation/mean) for diameter measurements in the SEM was greater than 10%.

The calibration data (Table II) follow the trend of the results presented by Li and Tietz [8] for cylindrical fibres of assorted materials with thicknesses ranging between 5 and 28 μm (Fig. 6). Linear regression on all the data plotted in Fig. 6 gives a correction of

$$d_{SEM}(\mu m) = 0.2805(\mu m) + 0.9367\ d_{laser}(\mu m) \quad (8)$$

with a coefficient of correlation [25] equal to 0.9994. This gives $d_{SEM} = d_{laser}$ at a thickness of approximately 4.4 μm: $d_{laser} > d_{SEM}$ above 4.4 μm, and $d_{laser} < d_{SEM}$ below 4.4 μm. If the regression is calculated for our data together with just the four thinnest fibres in the data of Li and Tietz, this cross-over occurs at 4.2 μm. However, regression on our data alone gives a cross-over at 1.8 μm, and the four thinnest fibres in the data of Li and Tietz give a cross-over at 3.2 μm. Thus, the cross-over diameter is highly sensitive to the accuracy of the calibration, and occurs in a range that substantially overlaps the range of diameters of our silk samples. The difference between d_{SEM} and d_{laser} in this range is not statistically significant.

We performed some additional SEM studies of major ampullate silk, to characterize further the variability in diameter. Four specimens were examined: two fibres silked at 10 cm s^{-1}, one fibre silked at 1 cm s^{-1}, and a segment of frame silk recovered from the web of a captive spider. Measurements were taken at five points along each fibre, separated by 1 mm intervals. The coefficients of variation were 2.91, 2.18, 7.38, and 5.47. Thus the variability cannot immediately be linked to forced silking. Cunniff *et al.* [26] also used SEM measurements to characterize diameters along major ampullate fibres silked at a variety of rates: 1.5, 3.1, 6.1, and 12.2 cm s^{-1}. Their data also do not reveal any trends in the variability or thickness of fibres as a function of silking rate.

TABLE II Calibration data for *N. clavipes* dragline: d_{eq} from laser diffraction (LD) versus diameter measured by scanning electron microscopy (SEM)

LD (μm)	LD S.D. (±μm)	SEM (μm)	SEM S.D. (±μm)
2.04	0.02	2.23	0.13
2.99	0.04	2.79	0.15
4.79	0.14	5.57	0.31
4.94	0.13	5.03	0.07
5.00	0.13	5.08	0.10

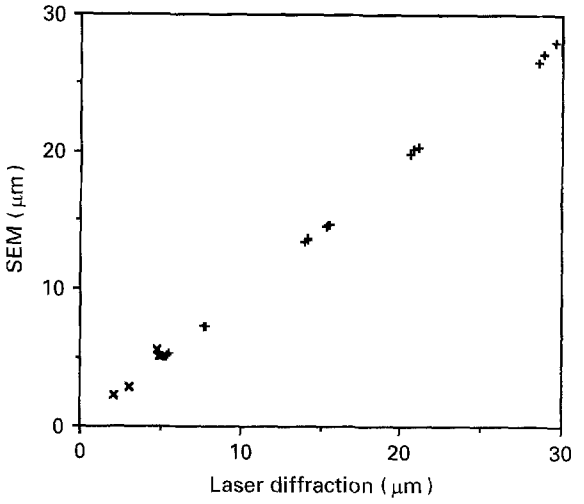

Figure 6 Calibration data for *N. clavipes* major ampullate silk (×), superimposed on the data published by Li and Tietz [8] (+) for thicker, cylindrical fibres of assorted materials.

There are several mechanisms by which spiders can influence the geometrical characteristics and physical properties of silk. First, spiders have muscles that can constrict the openings of their spinnerets to control the thickness of the fibre [27, 28]. Second, it has been inferred that spiders have a "holding brake" mechanism built into the spinneret to arrest their descent in the event of a fall [29]. It is likely that application of this brake will affect the silk locally. Third, the spiders are able to move their abdomens during the forced silking process. This motion (of the order of millimetres per second) adds to or subtracts from the nominal linear speed of drawing (10.3 cm s^{-1}). For this reason, it is desirable that we used a drawing speed that is significantly greater than the rate of natural silk spinning (approximately 1.1 cm s^{-1} [28]). The effects of these factors on the variability of silk diameter and cross-sectional shape are not known at present. Work [29] states that anesthetization (with CO_2) prevents any bodily movement, which suggests that silk collected from anesthetized spiders might be more uniform. However, the effects on the physiological processes of silk secretion and on the spinnerets are unknown, and there is evidence that the mechanical properties are degraded and that the variability in morphology and properties actually *increases* [19].

5. Conclusions

1. Laser diffraction can be used to measure an average local cross-sectional area of translucent fibres that are as thin as 2 μm in diameter. The average pertains to the length of fibre that intersects the beam. Measurements obtained by scanning electron microscopy can be used to calibrate the extent to which laser diffraction over- or under-estimates fibre diameter. The calibration factor for nearly cylindrical fibres is consistent with results obtained by previous authors for opaque, cylindrical fibres of diameter greater than 5 μm. The difference between diameters measured by laser diffraction and SEM is not statistically significant within the range exhibited by forcibly silked major ampullate fibres from mature *N. clavipes* spiders.

2. For the purpose of cross-sectional area measurement, fibres with an elliptical or oval cross-section can be treated as though the cross-section is circular. The maximum error is small, if the equivalent diameter of the circle is calculated from at least four measurements of apparent diameter (taken at equal intervals of fibre rotation through a 180° range), and if the axial (length to width) ratio of the cross-section is less than 1.5.

3. Non-cylindrical fibres that are twisted will exhibit cross-sectional ellipticities and areas that are smaller than those of twist-free fibres. Twisted fibres exhibit a pattern of bright and dark regions that alternate along their length in reflected light. The pattern can be used to deduce the extent to which the fibre is twisted.

4. Major ampullate fibres obtained from *Nephila clavipes* spiders have approximately elliptical cross-sections. The ellipticity fluctuates between 1 and 1.5, and the cross-sectional area is highly non-uniform. When such samples are tested for tensile properties, local cross-sectional area should be measured as close as possible to the region of eventual failure. Thicknesses calculated from the fibre denier will be unreliable.

Acknowledgements

We thank Dr D.B. Fischbach for stimulating conversations and the donation of equipment. This work was supported by the Donors of the American Chemical Society Petroleum Research Fund (grant 25218-AC), the National Science Foundation (grant BCS-9202007, jointly sponsored by the Division of Biological and Critical Systems and the Division of Materials Research), the US Army Research, Development and Engineering Center (Natick, MA; contract DAAK60-91-K-005), and the Whitaker Foundation.

Appendix. Cross-sectional area characterization based on measuring the "equivalent diameter" of an ellipse

Major ampullate silk from spiders is described as having an elliptical cross-section in a paper by Work [19]. As is sometimes the case in textbook descriptions [30] of textile fibres, the term "elliptical" appears to be colloquial rather than mathematically precise. However, the fact that our experimentally observed diffraction patterns in general are not symmetrical about the origin (see main text) confirms that the fibres do not typically have a circular cross-section. We therefore proceed with the ellipse as a more accurate representation of the fibre cross-section.

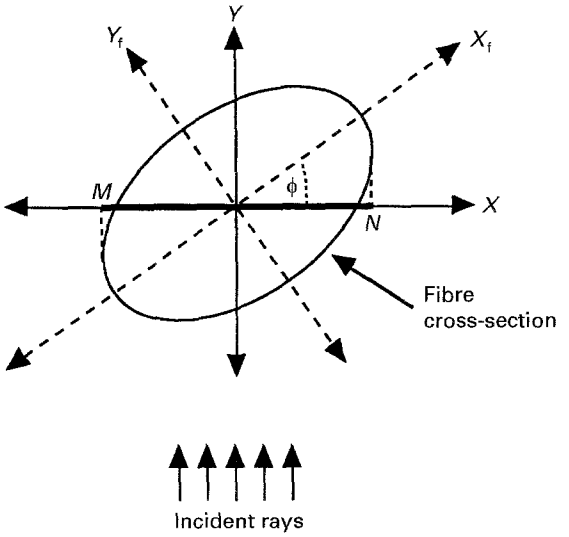

Figure A1 Schematic illustration defining laboratory axes, X, Y, the semi-major axes of an elliptical fibre cross-section, X_f, Y_f, and their relative orientation, ϕ. The apparent diameter of the fibre, as sampled by laser illumination incident parallel to Y, is $\overline{MN}$.

The major and minor axes of the elliptical cross-section define axes X_f and Y_f as shown in Fig. A1.

The standard (and simplest) equation for an ellipse is

$$\frac{x_f^2}{a^2} + \frac{y_f^2}{b^2} = 1 \tag{A1}$$

Transforming Equation A1 to the laboratory axes X and Y

$$x_f = x\cos\phi + y\sin\phi;\ y_f = -x\sin\phi + y\cos\phi \tag{A2}$$

$$\frac{(x\cos\phi + y\sin\phi)^2}{a^2} + \frac{(-x\sin\phi + y\cos\phi)^2}{b^2} = 1 \tag{A3}$$

To simplify the notation: substitute $c = \cos\phi$ and $s = \sin\phi$ in Equation A3

$$\frac{(cx + sy)^2}{a^2} + \frac{(-sx + cy)^2}{b^2} = 1 \tag{A4}$$

Treating the fibre as a two-dimensional slit (see Section 2), we note that the apparent diameter, $\overline{MN}$, of the fibre is equivalent to the projection of the fibre along Y on to the X-axis (Fig. A1). To obtain the length of $\overline{MN}$, it therefore is necessary to find the maximum and minimum values of x for the fibre orientation shown. One must therefore find $dx/dy = 0$, by differentiating Equation A4 with respect to y

$$\frac{2}{a^2}(cx + sy)\left(c\frac{dx}{dy} + s\right) + \frac{2}{b^2}(-sx + cy)\left(-s\frac{dx}{dy} + c\right) = 0 \tag{A5}$$

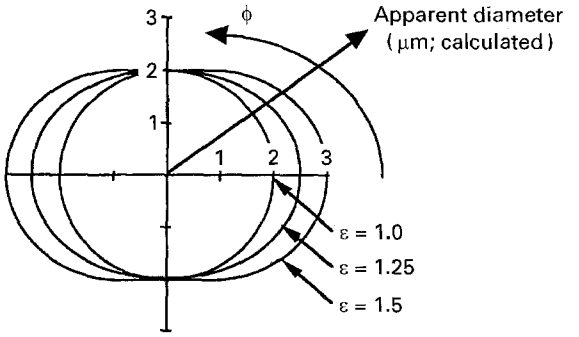

Figure A2 Polar plots of Equation A10 showing apparent diameter versus orientation for different values of ellipticity, ε. The smallest *radius* of each cross-section was normalized to unit length, i.e. $b = 1$, giving a smallest apparent diameter of 2 in each case. Note that these plots are not a direct representation of fibre cross-sections.

Setting $dx/dy = 0$ in Equation A5

$$\frac{s}{a^2}(cx + sy) + \frac{c}{b^2}(-sx + cy) = 0 \qquad \text{(A6)}$$

Rearranging Equation A6

$$y = \frac{csx(a^2 - b^2)}{a^2c^2 + b^2s^2} \qquad \text{(A7)}$$

Substituting Equation A7 in Equation A4 and solving for x, two solutions are obtained as required by symmetry

$$x = \pm(a^2\cos^2\phi + b^2\sin^2\phi)^{1/2} \qquad \text{(A8)}$$

The apparent diameter $\overline{MN}$ in Fig. A1 is therefore equal to

$$\overline{MN} = 2(a^2\cos^2\phi + b^2\sin^2\phi)^{1/2} \qquad \text{(A9)}$$

If ε denotes the ellipticity of the fibre, such that $a = \varepsilon b$, Equation A9 can be expressed as

$$\overline{MN} = 2b(\varepsilon^2\cos^2\phi + \sin^2\phi)^{1/2} \qquad \text{(A10)}$$

Polar plots of Equation A10 are shown in Fig. A2, to illustrate how the apparent diameter of an elliptical fibre varies as a function of ϕ and ε. In Fig. A2, ε ranges between 1 (for a cylindrical fibre) and 1.5 (the maximum value that we have observed in specimens of *N. clavipes* major ampullate silk). Although the plots for $\varepsilon > 1$ pertain to elliptical fibres, they are not themselves elliptical. Fig. A3 shows an experimentally determined polar plot of apparent diameter for a typical sample fibre; superimposed on the experimental data is a curve generated by setting $\varepsilon = 1.45$ in Equation A10, scaled and rotated to a corresponding orientation. Thus, the fibre is demonstrated to have an approximately elliptical cross-section.

For the purpose of area calculation, we use apparent diameters to define the "equivalent diameter" of the elliptical cross-section as

$$d_{eq} = \sum_{j=0}^{j\frac{1}{k}=k-1} 2b\left[\varepsilon^2\cos^2\left(\delta_0 + j\frac{180°}{k}\right) + \sin^2\left(\delta_0 + j\frac{180°}{k}\right)\right]^{1/2} \qquad \text{(A11)}$$

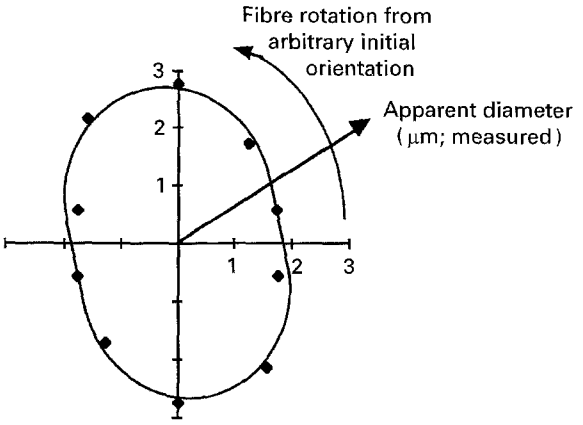

Figure A3 Values of apparent diameter measured by laser diffraction for a major ampullate silk fibre, plotted as a function of fibre rotation. The fitted curve was generated by setting $\varepsilon = 1.45$ (and $b = 1$) in Equation A10, and then rotating and linearly scaling the resultant polar plot to superimpose on the experimentally measured data.

(The apparent diameter $\overline{MN}$ is measured k times, with the initial fibre rotation defining $\phi = \delta_0$, and with the fibre being rotated through an additional $\delta = 180°/k$ between successive measurements.) A circular cross-section assigned the diameter d_{eq} will have an area of

$$A_{eq} = \frac{\pi d_{eq}^2}{4} = \frac{\pi b^2}{k^2}\left\{\sum_{j=0}^{j=k-1}\left[\varepsilon^2\cos^2\left(\delta_0 + j\frac{180°}{k}\right) + \sin^2\left(\delta_0 + j\frac{180°}{k}\right)\right]^{1/2}\right\}^2 \qquad \text{(A12)}$$

The corresponding elliptical cross-section will have an area of

$$A_{el} = \pi ab = \pi\varepsilon b^2 \qquad \text{(A13)}$$

Thus the fractional error due to calculating cross-sectional area from an equivalent diameter, versus finding an elliptical cross-section that best fits the experimental diameter measurements, is given by

$$\frac{A_{eq} - A_{el}}{A_{el}} = \frac{1}{\varepsilon k^2}\left\{\sum_{j=0}^{j=k-1}\left[\varepsilon^2\cos^2\left(\delta_0 + j\frac{180°}{k}\right) + \sin^2\left(\delta_0 + j\frac{180°}{k}\right)\right]^{1/2}\right\}^2 - 1 \qquad \text{(A14)}$$

The error is therefore a function of ε, k, and δ_0. For fixed values of ε and k, Equation A14 was evaluated as a function of δ_0 to determine which initial fibre orientation gives the largest error in each case. The values of δ_0 so identified were used to construct Fig. A4, which shows the maximum error as a function of fibre cross-sectional ellipticity, and how this depends on the number of diameter measurements. The maximum overestimation of area is seen to be an increasing function of ellipticity; also, its dependence on the number of diameter measurements taken around the fibre is insignificant, *provided that at least four measurements are taken* at equal intervals of fibre

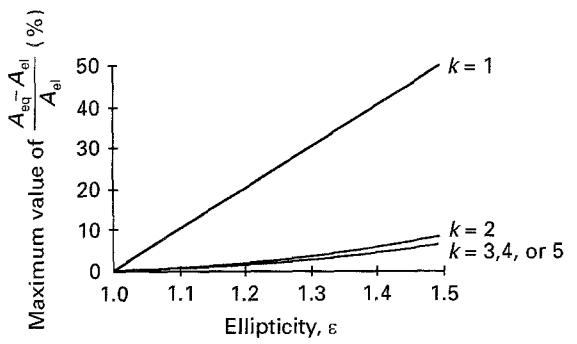

Figure A4 Plots of maximum overestimation of cross-sectional area versus ellipticity, developed from Equation A14 for several values of k. The curves for $k \geq 3$ cannot be distinguished over the plotted domain $1.0 \leq \varepsilon \leq 1.5$ at this scale.

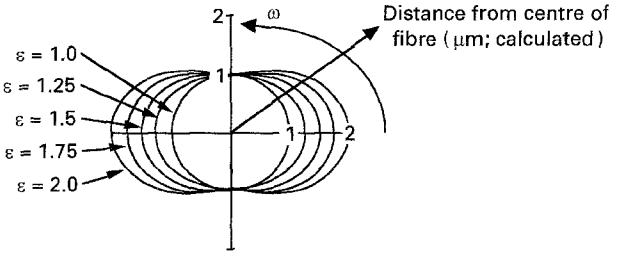

Figure A5 Polar plots of Equation A16, describing a circular fibre cross-section ($\varepsilon = 1$), two oval cross-sections ($\varepsilon = 1.25$ and 1.5), and two "dog-bone" cross-sections ($\varepsilon = 1.75$ and 2.0). The smallest radius of each cross-section was normalized to unit length, i.e. $b = 1$.

rotation in the range $\phi = \delta_0$ to $\phi = \delta_0 + 180°$. While calculating cross-sectional area from an equivalent diameter is faster and simpler than finding an elliptical cross-section that best fits the experimental diameter measurements, the maximum overestimation of area introduced by this expedient is small.

We recognize that, while the silk fibre cross-sections are represented closely by ellipses, there is no a priori reason to *expect* an elliptical cross-section. When synthetic textile fibres are dry-spun from solution, they may develop an oval or (at higher axial ratios in thicker fibres) a "dog-bone" cross-section, as a result of the initial formation of a rigid "skin" around the solidifying material [31, 32]. Because natural silk is also produced from solution by dry-spinning, one could expect a similar evolution of cross-section as the material dries (though silk, being thinner, does not lose sufficient volume of solvent to collapse to a "dog-bone"). Families of oval cross-sectional profiles are generated by the equations

$$(x_f^2 + y_f^2)^p = ax_f^2 + by_f^2$$

(rectangular co-ordinates; $p > 1$)

or

$$r = (a\cos^2\omega + b\sin^2\omega)^{\frac{1}{2p-2}} \text{ (polar co-ordinates)} \quad \text{(A15)}$$

Simple cases are obtained by setting $p = 3/2$ in Equation A15

$$r = a\cos^2\omega + b\sin^2\omega$$

$$= b(\varepsilon\cos^2\omega + \sin^2\omega) \quad \text{(A16)}$$

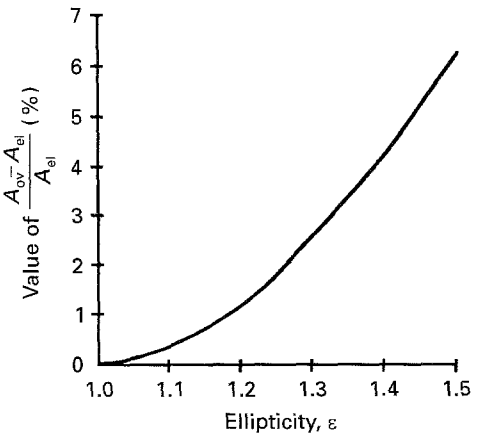

Figure A6 Plot of overestimation of cross-sectional area versus ellipticity, obtained from Equation A19.

Plots of Equation A16 are shown in Fig. A5, illustrating how the profile depends on ε. While our studies of major ampullate silk suggest that $1 \leq \varepsilon < 1.5$, Fig. A5 includes the profiles for $\varepsilon = 1.75$ and 2.0 in order to show that Equation A16 would be consistent with evolution of a "dog-bone" cross-section in thick fibres.

The area, A_{ov} of the ovals generated by Equation A16 can be calculated as follows [33]

$$A_{ov} = 4\int_0^{\pi/2} \frac{1}{2}[r(\omega)]^2\,d\omega$$

$$= 2\int_0^{\pi/2} [b(\varepsilon\cos^2\omega + \sin^2\omega)]^2\,d\omega \quad \text{(A17)}$$

Integration of Equation A17 yields

$$A_{ov} = \frac{\pi}{8}b^2(3\varepsilon^2 + 2\varepsilon + 3) \quad \text{(A18)}$$

The fractional difference in area between such an oval and an ellipse having the same axial ratio can be determined from Equations A13 and A18

$$\frac{A_{ov} - A_{el}}{A_{el}} = \frac{3\varepsilon^2 - 6\varepsilon + 3}{8\varepsilon} \quad \text{(A19)}$$

This function is plotted as Fig. A6. For any value of ε in the range exhibited by our major ampullate silk fibres

$$\frac{A_{ov} - A_{el}}{A_{el}}\text{(Fig. A6)} \approx \frac{A_{eq} - A_{el}}{A_{el}}\text{(Fig. A4)} \quad \text{(A20)}$$

provided that the equivalent diameter is calculated from at least four measurements taken at equal intervals of fibre rotation in the range $\phi = \delta_0$ to $\phi = \delta_0 + 180°$. This correspondence supports Fig. A4 as a realistic representation of the error that arises when we use an equivalent diameter to calculate the cross-sectional area of fibres.

References

1. J. M. GOSLINE, M. E. DEMONT and M. W. DENNY, *Endeavour* **10** (1986) 37.
2. J. C. ZEMLIN, "A study of the mechanical behavior of spider silks", Report 69-29-CM (AD 684333) (US Army Natick Laboratories, Natick, MA, 1968).

3. C. VINEY, in "Structure, Cellular Synthesis and Assembly of Biopolymers", edited by S.T. Case (Springer, Heidelberg, 1992) p. 255.
4. M. W. DENNY, *J. Exp. Biol.* **65** (1976) 483.
5. B. L. THIEL, D. D. KUNKEL and C. VINEY, *Biopolymers* **34** (1994) 1089.
6. R. W. WORK, *Textile Res. J.* **47** (1977) 650.
7. R. MORETON, *Fibre Sci. Technol.* **1** (1969) 273.
8. C.-T. LI and J. V. TIETZ, *J. Mater. Sci.* **25** (1990) 4694.
9. P. GAGNAIRE, P. DELHAES and A. PACAULT, *J. Chim. Phys.* **84** (1987) 1407.
10. A. J. PERRY, B. INEICHEN and B. ELIASSON, *J. Mater. Sci.* **9** (1974) 1376.
11. M. A. FADEL, W. H. OSMAN, F. M. TERA and N. A. ABDEL-ZAHER, *Polym. Degrad. Stabil.* **19** (1987) 343.
12. D. B. FISCHBACH and P. M. LEMOINE, *Compos. Sci. Technol.* **37** (1990) 55.
13. R. S. LONGHURST, "Geometrical and Physical Optics" (Longmans, London, 1967).
14. S. R. POWERS and D. J. SOMERFORD, *Opt. Commun.* **26** (1978) 313.
15. *Idem, J. Phys. D Appl. Phys.* **12** (1979) 1809.
16. R. G. GREENLER and J. W. HABLE, *Am. Sci.* **77** (1989) 169.
17. I. M. FOUDA and M.M. EL-TONSY, *J. Mater. Sci.* **25** (1990) 4752.
18. E. IIZUKA, *Biorheology* **3** (1965) 1.
19. R. W. WORK, *Textile Res. J.* **46** (1976) 485.
20. W. S. BICKEL, W. GILLIAR and B. BELL, *Appl. Optics* **19** (1980) 3671.
21. R. W. WORK and P. D. EMERSON, *J. Arachnology* **10** (1982) 1.
22. M. A. BECKER and N. TUROSS, in "Silk Polymers: Materials Science and Biotechnology", edited by D. L. Kaplan, W. W. Adams, B.L. Farmer and C. Viney (American Chemical Society, Washington DC, 1994) p. 252.
23. L. S. WATKINS, in "Lasers in Industry", edited by S. S. Charschan (Van Nostrand Reinhold, New York, 1972) p. 367.
24. R. W. WORK and N. MOROSOFF, *Textile, Res. J.* **52** (1982) 349.
25. M. KURTZ, "Handbook of Applied Mathematics for Engineers and Scientists" (McGraw-Hill, New York, NY, 1991).
26. P. M. CUNNIFF, S. A. FOSSEY, M. A. AUERBACH and J. W. SONG, in "Silk Polymers: Materials Science and Biotechnology", edited by D. Kaplan, W. W. Adams, B. Farmer and C. Viney (American Chemical Society, Washington, DC, 1994) p. 234.
27. R. S. WILSON, *Q. J. Microsc. Sci.* **103** (1962) 549.
28. R. F. FOELIX, "Biology of Spiders" (Harvard University Press, Cambridge, MA, 1982).
29. R. W. WORK, *Trans. Am. Microsc. Soc.* **97** (1978) 180.
30. F. W. BILLMEYER, "Textbook of Polymer Science" (Wiley, New York, 1984).
31. J. CORBIÉRE, in "Man-Made Fibers: Science and Technology", edited by H. F. Mark, S. M. Atlas and E. Cernia (Wiley, New York, 1967) p. 133.
32. A. ZIABICKI, "Fundamentals of Fibre Formation" (Wiley, London, 1976).
33. S. LANG, "A First Course in Calculus" (Addison-Wesley, Reading, MA, 1973).

Received 7 March 1994
and accepted 3 February 1995